

広角ダブルレットメタレンズに於ける誘電体メタサーフェス素子の種類の違いによる影響

鳥羽英光, 高木英嗣, 大橋道雄, 大滝 桂, 瀧川雄一

Influence on Wide-Angle Doublet Metalenses Due to Different Types of All-Dielectric Metasurfaces[†]

Hidemitsu TOBA, Hidetsugu TAKAGI, Michio OHASHI, Katsura OTAKI and Yuichi TAKIGAWA

ダブルレットメタレンズは、約30度の入射角度まで回折限界の集光が可能であることが先行文献で示されている。この結果は、メタレンズが斜め入射でも有効に機能することを示している。また、様々なメタアトムが提案されているが、どのようなメタアトムが斜め入射に強いかを比較した報告は私たちの知る限りない。そこで我々はまず、3種類のメタアトムの入射角依存性を数値的に計算した。その結果、導波路型構造が斜め入射に対して最もロバストであることがわかった。次に、円筒形ダブルレットメタレンズについて電磁場シミュレーションを行い、マイクロポスト型と導波路型の比較を行った。これらの結果から、導波路型メタサーフェスは、先行文献のダブルレットレンズの性能をさらに向上させる可能性があることが分かった。

It has been shown in previous literature that nearly diffraction limited focusing is possible by a doublet metalens up to almost 30 deg. This result indicates that metalenses can work well, even at oblique incidence. Although various meta-atoms have been proposed, as far as we know, there is no report that compares what kind of meta-atom is robust against oblique incidence. Here, we first numerically calculated the incident angle dependence of the three types of meta-atoms. The results show that the waveguide-type structure is the most robust to oblique incidence. Next, we performed rigorous electromagnetic simulations for the cylindrical doublet metalenses to compare the micropost-type and waveguide-type. These results indicate that a waveguide-type metasurface further improves the off-axis performance of the doublet lens previously introduced.

Key words メタサーフェス, メタレンズ, 入射角度依存性
metasurface, metalens, incident angle dependence

1 Introduction

Metasurfaces are 2D arrays of subwavelength structures known as “meta-atoms.” Metasurfaces have been shown to enable control of the amplitude, phase, polarization, and orbital angular momentum of reflected or transmitted light. One of the important applications of metasurfaces is wavefront control and especially the metasurface that works as a metalens. Many kinds of meta-atoms have been designed for the phase control of metasurfaces using high-index materials. Lalanne and Chavel classified them into three groups [1]: waveguide-type, resonant-type micropost, and resonant-type nanodisk. The waveguide-type has a single mode in the structure. The period is smaller than the structural cutoff [2]

and the aspect ratio is relatively high. Microposts are multi-mode; Kamali *et al.* reported that at least eight resonant modes contribute to the transmittance and the phase in their micropost [3]. The aspect ratio is weakly relaxed compared to the waveguide-type. The doublet metalens that we focus on in this paper is a micropost-type structure. A nanodisk-type can be understood in terms of Mie resonance [4], [5]. A nanodisk-type metalens consists of periodically arranged disk-like structures whose fundamental electric and magnetic resonances coincide at the same wavelength. The aspect ratio is significantly relaxed and good for manufacturing. The three groups classified by Lalanne and Chavel are simple structures such as square pillars or cylindrical pillars that are polarization-independent for normal incident light

[†] This paper is reprinted with permission from © Optica Publishing Group of reference [21].

due to their symmetry. Most metalenses are designed for a normal incident beam. However, oblique incident light is important for many applications such as imaging. Arbabi *et al.* showed that doublet metalenses are capable of nearly diffraction-limited focusing up to an incidence angle of 30 deg [6]. Their results indicate that the subwavelength elements designed by Arbabi *et al.* are robust to the oblique incidence. However, the paper does not mention much about oblique incidence characteristics.

Although there are previous studies on the characteristics of oblique incidence on dielectric metasurfaces [1], [7], [8], there is no report, to the best of our knowledge, that compares the phase responses of oblique incidence and how those three types affect lens performances. In this paper, we first calculate the incident angle dependence of the three types of meta-atoms classified by Lalanne and Chavel. Our results indicate that the waveguide-type can be most suitable for wide-angle incidence. We then confirm the effect of structural differences on the performance of a doublet lens with full electromagnetic simulations. There are studies on the optimization of the metasurface for further efficiency improvement [9]–[11], but optimized structures are not covered in this paper.

2 Oblique Incidence Characteristics of The Meta-Atoms

We calculate the transmission characteristics of three types of meta-atoms by rigorous coupled-wave analysis

(RCWA) [12], [13]. The angle of incidence is calculated from 0 deg to 30 deg. The transmittance and phase are calculated for both TE and TM polarization for oblique incidence because the response of the structure is different depending on the polarization, even when the structure is polarization independent at normal incidence. For each type, the parameters of the metasurface structure, such as height of the pillar and period, are selected from previous papers. The parameters used in the calculation are summarized in Table 1. Fig. 1 illustrates the dependence on the angle of incidence for the three types of subwavelength elements with TM polarization, and Fig. 2 shows the same for TE polarization. Figs. 1 (a) and 1 (d) are the results for the transmittance and the phase of the waveguide-type [2], respectively. Similarly, Figs. 1 (b) and 1 (e) and Figs. 1 (c) and 1 (f) are those of the micropost-type [6] and the nanodisk-type [5]. The

Table 1 Parameters for Oblique Incidence Characteristic Calculations

Meta-atom Type	Waveguide	Micropost	Nanodisk
Lattice type	Square	Hexagonal	Square
Lattice const.	272 nm	450 nm	666 nm
Pillar shape	Square	Cylindrical	Cylindrical
Pillar height	817 nm	600 nm	220 nm
Pillar material	TiO ₂	Amorphous silicon	Silicon
Wavelength	633 nm	850 nm	1340 nm
Material between pillars	Air	SU-8	Embedded in medium with $n = 1.66$
Substrate	SiO ₂	SiO ₂	
References	[2]	[6]	[5]

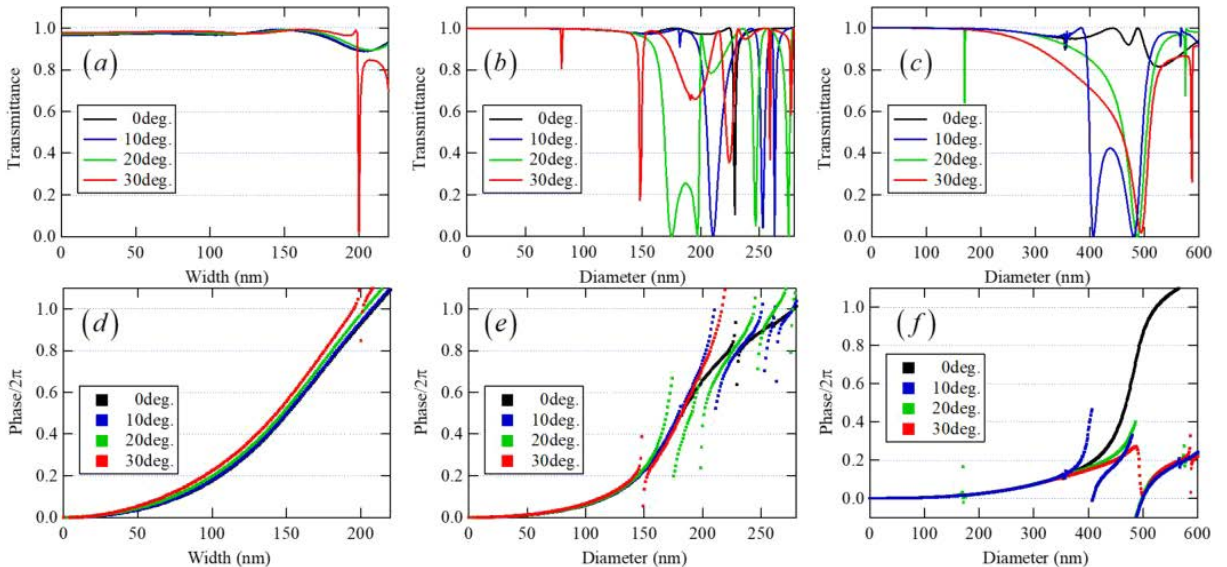


Fig. 1 Incident angle dependence of the transmission coefficient from an infinite 2D array of meta-atoms for TM polarized light: (a)–(c) Transmission coefficients and (d)–(f) phase. (a), (d) Waveguide-type structure [2]. (b), (e) Micropost structure [6]. (c), (f) Nanodisk structure [5].

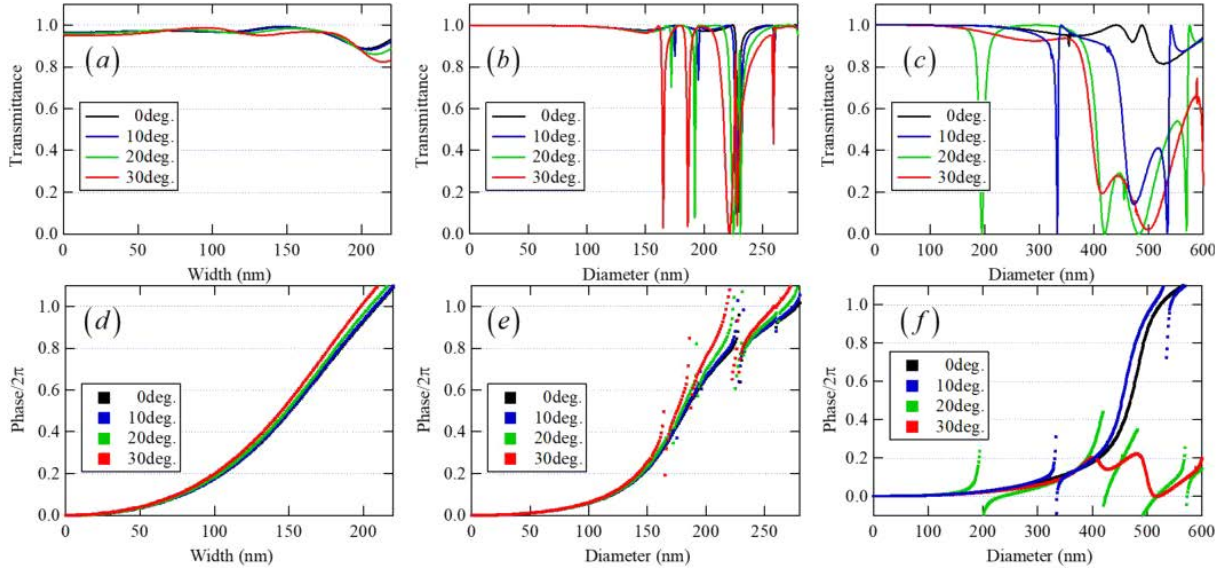


Fig. 2 Incident angle dependence of the transmission coefficient from an infinite 2D array of meta-atoms for TE polarized light: (a)–(c) Transmission coefficients and (d)–(f) phase. (a), (d) Waveguide-type structure [2]. (b), (e) Micropost structure [6]. (c), (f) Nanodisk structure [5].

same applies to Fig. 2 regarding the numbering of subfigures.

The desired features of a meta-atom for lens applications are that the transmittance of the metasurface is close to unity and that the phase covers the range of 2π or more by changing the width of the pillars. Further, it is required that the phase does not change with angle of incidence. In the case of normal incidence, it can be seen in Fig. 1 and Fig. 2 that the phase can be controlled over a range larger than 2π and with high transmittance for all three types. For the micropost-type and the nanodisk-type, however, there are large drops in the transmittance when the incidence angle is 20 deg and 30 deg. These drops are considered to originate from the multiple resonances because multiple resonances can cause destructive interferences. Furthermore, the phases around the drops in transmittance are drastically modulated. Therefore, these will not work well at oblique incidence. In particular, the nanodisk-types cannot cover 2π by changing the diameter at incident angles greater than 10 deg. This is due to the fact that the electrical resonance and magnetic resonance in the nanodisk no longer overlap at oblique incidence, which is clearly seen when the incidence angle is 10 deg in Figs. 1 (c) and 1 (f). Therefore, metalenses made from nanodisks will not have sufficient phase modulation at oblique incidence and good lens performance cannot be expected. On the other hand, the waveguide-type has almost the same transmission phase as normal incidence up to 30 deg. Because the waveguide-type has only a single mode in the structure, the destructive interferences do not

happen, even at oblique incidence [7]. These results indicate that the waveguide-type can be superior to the lens performance compared to the other types. Fig. 3 shows examples of the electromagnetic field distributions for the incident angles 0 deg and 20 deg for each type. The electromagnetic field distribution in the waveguide for incident angle 20 deg is almost the same as that of normal incidence because of the single mode; on the other hand, the electric field distributions at 20 deg in the micropost-type and nanodisk-type evidently differ from those at normal incident lights because of multimode.

The doublet metalenses introduced in [6] worked well for oblique incident beams composed of the micropost-type meta-atom. However, from the results of these oblique incident characteristics, it is possible that the performance of the doublet metalenses is further improved by using the waveguide-type instead of the micropost-type.

Since these transmission and phase simulations do not directly indicate what kind of lens performance improvement should be expected, we performed lens-focusing simulations to find out.

3 Electromagnetic Simulations for Cylindrical Doublet Metalens

To understand what kinds of lens performance the waveguide-type improves, we simulate focusing with doublet-metalenses composed of micropost-type and waveguide-type meta-atoms by full electromagnetic simulations. The former

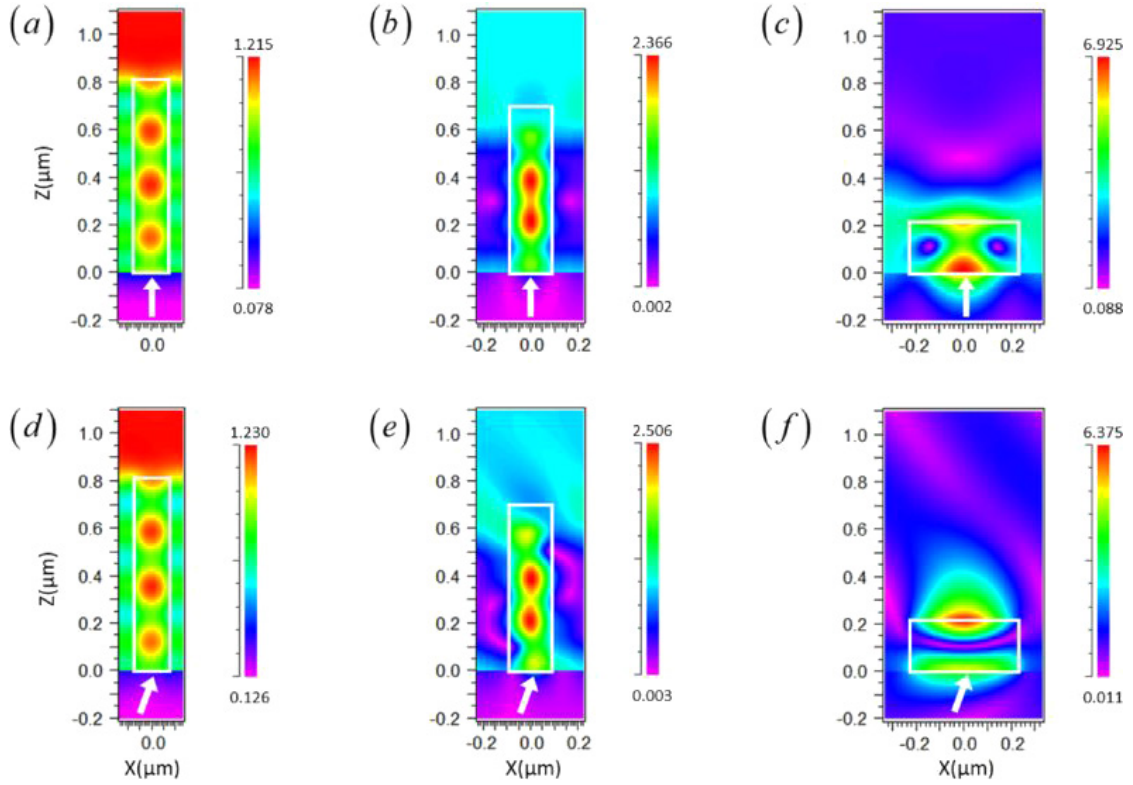


Fig. 3 Examples of the electromagnetic field amplitudes E_y for TE polarized light at $Y = 0$. (a)–(c) Normal incidence and (d)–(f) incident angle 20 deg. (a), (d) Waveguide-type structure [2] of pillar width 150 nm. (b), (e) Micropost structure [6] of diameter 180 nm. (c), (f) Nanodisk structure [5] of diameter 460 nm. The electronic field component of the incident wave is omitted. Arrows indicate the angle of incidence.

Table 2 Parameters for Oblique Incidence Characteristic Calculations

Meta-atom Type	Waveguide	Micropost
Lattice type	Square	Hexagonal
Lattice const.	280 nm	450 nm
Pillar shape	Cylindrical	Cylindrical
Pillar height	800 nm	600 nm
Material	Amorphous silicon	Amorphous silicon
Wavelength	850 nm	850 nm
Material between pillars	Air	SU-8
Substrate	SiO ₂	SiO ₂

is a micropost-type introduced by Arbabi *et al.* [6] and the latter is a waveguide-type that we designed for these cylindrical lens simulations. Table 2 shows the parameters. The diameter used in the cylindrical lens simulations is from 91 nm to 190 nm and the maximum aspect ratio is 8.8. Fig. 4 is the pillar width dependence of the transmittance and the phase for the waveguide-type structure for normal incidence. The inset of the graph in Fig. 4 is a schematic illustration of the unit cell of the meta-atom. The amorphous silicon cylindrical pillars are aligned periodically on a 2D square lattice

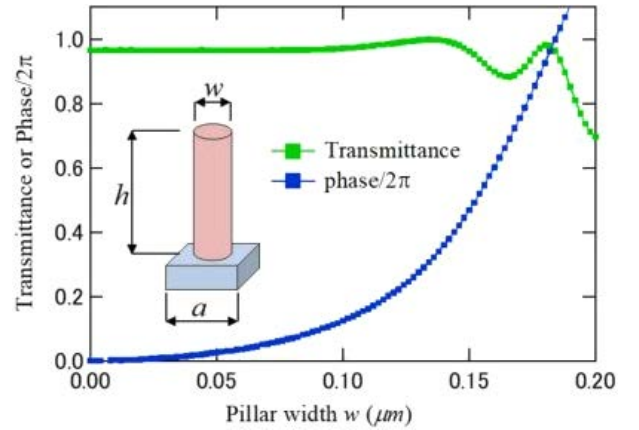


Fig. 4 Transmittance and the phase of the waveguide-type meta-atom we used in the doublet simulations.

on the fused silica substrate with a height of $h = 800 \text{ nm}$ and a lattice constant $a = 280 \text{ nm}$. In our simulations, we use the design of the doublet metalens introduced by Arbabi *et al.*, whose phase profile parameters are shown in Table 1 of the supplementary material in [6]. The cross section is depicted in Fig. 5. The doublet metalens consists of two flat lenses. We refer to the first one as a correcting lens and the second one as a focusing lens. This doublet lens is designed for a single wavelength of 850 nm.

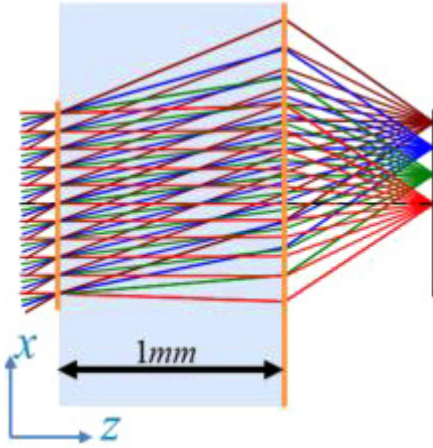


Fig. 5 Doublet metalens introduced by Arbabi *et al.* Phase profile parameters for this doublet metalens are shown in Table 1 in the supplementary material in [6].

There are various electromagnetic simulation methods to study the behavior of electromagnetic fields in structures of the order of wavelength size or below. In particular, the finite-difference time-domain (FDTD) method [14], [15] and the RCWA is widely used. The RCWA is most typically applied to solve scattering from periodic structures. Therefore, we chose RCWA to calculate the transmittance and phase of the periodic element of a metasurface for Figs. 1 and 2. On the other hand, FDTD is more flexible than RCWA, and FDTD can be used for a nonperiodic structure, so we chose FDTD for the doublet metalens simulations below. FDTD grid element sizes are typically from $1/10$ to $1/20$ of the wavelength to avoid numerical dispersion. However, the grid size to simulate a metalens must be much smaller to represent the change of the pillar diameter of the meta-atom in metasurfaces and a much larger scale simulation is required. As a result, a tremendous amount of time and PC memory will be required to simulate a metalens of a size for practical use. In this paper, we simulate the doublet metalens designed by Arbabi *et al.* [6] (see Fig. 5). The diameter of the lens is $\phi = 1.6 \text{ mm}$ and the thickness is $t = 1 \text{ mm}$. If we simulate such a double metalens by simple FDTD with a 5 nm grid element size, the simulation requires $320,000 \times 320,000 \times 200,000$ grid elements. This means that we need much more than petabyte memories to simulate the doublet metalens—and it is unrealistic.

There are several ways to simulate the mm size doublet lens and avoid this difficulty. One approach is to proportionally reduce the simulation size [16]. Lenses under those kinds of simulations are scaled by some scaling factor with parameters such as NA or F/no kept constant. It is reasonable to assume that the focusing features are unchanged

because the spot size for ideal focusing depends only on the wavelength and the NA. However, the wavefront aberrations are proportional to the scaling factor and, in this situation, the wavefront aberrations will be underestimated and the balance between the wavefront aberration and the other effects will change. Hence, the lens should be simulated in the same scale as we use in practice, if we want to know the imaging quality in terms of the aberration. Another approach is that the metalens is treated as a phase mask. The response at each position on the metalens is defined by the transmittance and its phase obtained by numerical calculation of individual elements [17]. This method allows us to efficiently simulate many features of the metalenses. However, interactions between subwavelength elements are neglected in this method. In the dielectric meta-surface, a material with a high refractive index is used for the meta-atom so that the electromagnetic field is localized in the meta-atoms and the interactions between neighboring meta-atoms are suppressed to a small level. Therefore, the assumption that the meta-atom can be treated as an independent element might hold to some extent, but the interaction is not zero. In particular, the interaction is likely to be very different at regions where the phase changes rapidly. Byrnes *et al.* proposed another good method that takes advantage of the fact that the phase profile away from the center of the lens can be approximated as a collection of deflector cells [9]. The propagation components from each cell are obtained by RCWA and then the electric fields immediately after transmission through the lens are constructed by the components. This method can calculate a large lens with a good approximation, but the complicated calculations are then required when the incident light is not a simple plane wave, as is the case at the focusing lens of the doublet metalens.

We adopt yet another approach. We simulate a cylindrical lens instead of a rotationally symmetric aspherical lens [18]. Fig. 5 can be considered as the cross section of the corresponding cylindrical lens as well as that of the rotationally symmetric aspherical lens and the wavefront profile on the meridional plane of the spherical lens is identical to the wavefront profile for the cylindrical lens. In a cylindrical lens simulation, we can only know the behavior of the wave on the meridional plane, but the balance between the wavefront aberration and the other effects are the same as in the original lens and we can get useful information from the results. Because the meta-atoms on the cylindrical metalenses are aligned periodically along the cylindrical axis, we can use a periodic boundary condition. And the periodic lat-

tice constants of meta-atoms are smaller than the wavelength. This means that a cylindrical lens configuration can reduce the simulation size smaller than the wavelength along the cylindrical axis. In the case of a doublet metalens, however, the distance between the two metalenses is as large as 1 mm. Hence, even if there is a cylindrical configuration with a periodic boundary condition, the simulation size is still too large to simulate along the optical axis. We must therefore adopt an additional means to reduce the calculation time. One of the ways to reduce the calculation size is subgridding [15]. The space between the two metalenses of the doublet is a uniform medium and the grid element size can be larger than needed by metasurface elements. Still, the calculation size with subgridding remains huge. So instead of subgridding, we calculate the propagation from the first metalens surface to the second with Rayleigh–Sommerfeld (RS) diffraction that is usually used for scalar diffraction. The medium between the first metalens and the second one is isotropic, homogeneous, and source free. Each six components of the electromagnetic field obey the RS diffraction formula independently in the medium (see Appendix A). Therefore, an exact full electromagnetic solution can be calculated by the RS diffraction between the two metalenses. Then the FDTD calculation is needed only in the vicinity of the two metalenses and the calculation size along optical axes becomes only several micrometers if the wavelength used in the simulations is 850 nm. As described above, by adopting a combination of an RS diffraction calculation and FDTD with a cylindrical lens configuration, it is possible to perform the imaging simulation of the doublet lens in a realistic time. We calculate the fields on the focal plane by following steps:

Step 1: FDTD calculation for the correcting lens.

Input plane wave is excited in the plane just before the correcting lens. The outputs are E_x , E_y , H_x , and H_y in the plane just after the correcting lens.

Step 2: RS diffraction calculation between correcting lens and focusing lens.

Calculate the RS diffraction for each field distribution outputted by FDTD calculation in Step 1. The outputs of these diffraction calculations are the field distributions just before the focusing lens. These calculations can be calculated independently for each field.

Step 3: FDTD calculation for the focusing lens.

Input source is excited in the plane just before the focus-

ing lens using the field distributions calculated by RS diffraction in Step 2. Outputs are E_x , E_y , H_x , and H_y in the plane just after the focusing lens, just like in Step 1.

Step 4: RS diffraction calculation from focusing lens to focal plane.

Calculate the RS diffraction as in Step 2 from the plane just after the focusing lens to the focal plane. The focal spot and the modulation transfer function (MTF) can be calculated from the outputs.

It is important to note that the multiple reflections between the two metalenses do not appear in the results since the back-ward wave is excluded from the calculation of the RS diffraction in Step. 2. However, if there is 10% reflection from a metasurface, noise originated from the multiple reflections will be only about 1% and there will be no significant effect on the simulation results. Multiple reflections will be discussed further at the end of Section 4.

We adopt the FFT–DI method [19] to numerically calculate the RS diffraction formula. The sampling periods and the calculation size on the input plane do not change at the output plane and the output region can be shifted perpendicular to the optical axis by shifting the center of the transfer function kernel $h(x, y)$ in Eq. (A3) of the FFT–DI calculation. In our calculations, since the structures along the cylindrical axis are smaller than the wavelength, propagated wave fields (not evanescent wave fields) are constant along the cylindrical axis. Therefore, we adopt as the transfer function kernel Eq. (A3) instead of Eq. (A2) for the cylindrical doublet metalenses simulations.

4 Results and Discussion

Here, we show the simulation results of the doublet metalenses made of micropost-type and waveguide-type meta-atoms. Simulations are performed with both TM and TE polarization, and the incidence angles are from 0 deg to 30 deg in 10 deg steps. The grid size in the FDTD simulation is $\Delta x = \Delta y = \Delta z = 5 \text{ nm}$. Perfectly matched layers (PML) are used in the Z axis direction and the periodic boundary conditions are used in the X axis and Y axis directions.

Fig. 6 and 7 show focal spots on the focal plane at 0 deg, 10 deg, 20 deg, and 30 deg incident angles, and the corresponding MTF. Fig. 6 is for TM polarization and Fig. 7 is for TE polarization. Figs. 6 (a) and 6 (c) shows the focal spots for the micropost-type and waveguide-type, respectively. Figs. 6 (b) and 6 (d) are the MTFs. The same applies to

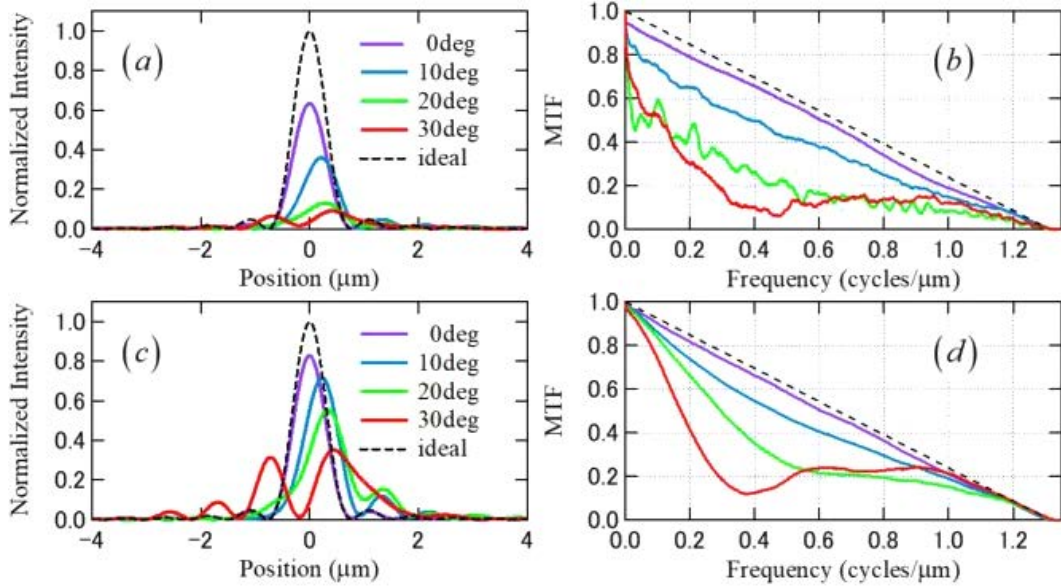


Fig. 6 Focal spots and MTFs for TM polarization: (a) Focal spots of micropost-type, (b) MTF for micropost-type, (c) focal spot of waveguide-type, and (d) MTF for waveguide-type. Dotted line represents ideal focal spot and the corresponding MTF.

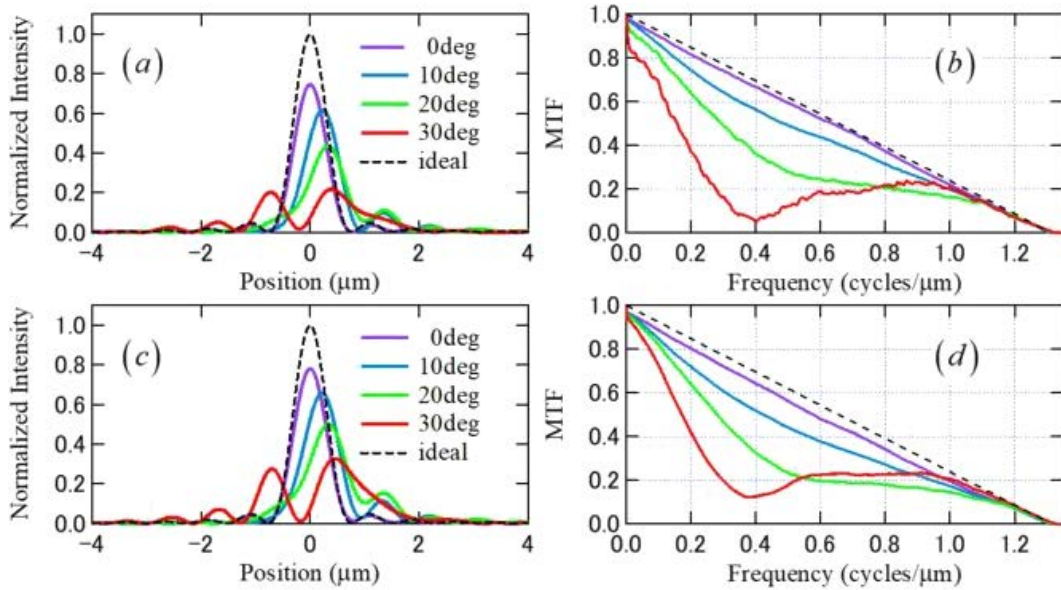


Fig. 7 Focal spots and MTFs for TE polarization: (a) Focal spots of micropost-type, (b) MTF for micropost-type, (c) focal spot of waveguide-type and (d) MTF for waveguide-type. Dotted line represents ideal focal spot and the corresponding MTF.

Fig. 7 regarding the numbering of subfigures. Intensity distributions are calculated by $I = |S_z| = |E_x H_y - E_y H_x|$ and are normalized so that the maximum value of an ideal spot without loss due to scattering or reflection is unity. The chief ray heights calculated by ray tracing are set at the origin of the horizontal axis for oblique incident focal spots.

The difference between the results of the micropost-type and those of the waveguide-type is not large for the TE polarized incident light. Similarly, the difference in results is not large in the case of normal incidence for TM polariza-

tion. However, we can see differences in the MTF between the two types at low frequencies below 0.2 cycles/ μm for the oblique incidence, especially at 20 deg and 30 deg of TM polarization. Obviously, the waveguide-type is superior to the micropost-type. Moreover, the MTF for incident angles of 20 deg and 30 deg of the micropost-type is very noisy. This is because speckle-like noise is distributed around the spot. Note that the intensities of the speckle are too small to be seen in Fig. 6 (a). We can understand it from the viewpoint that the MTF is defined as the magnitude of the Fourier

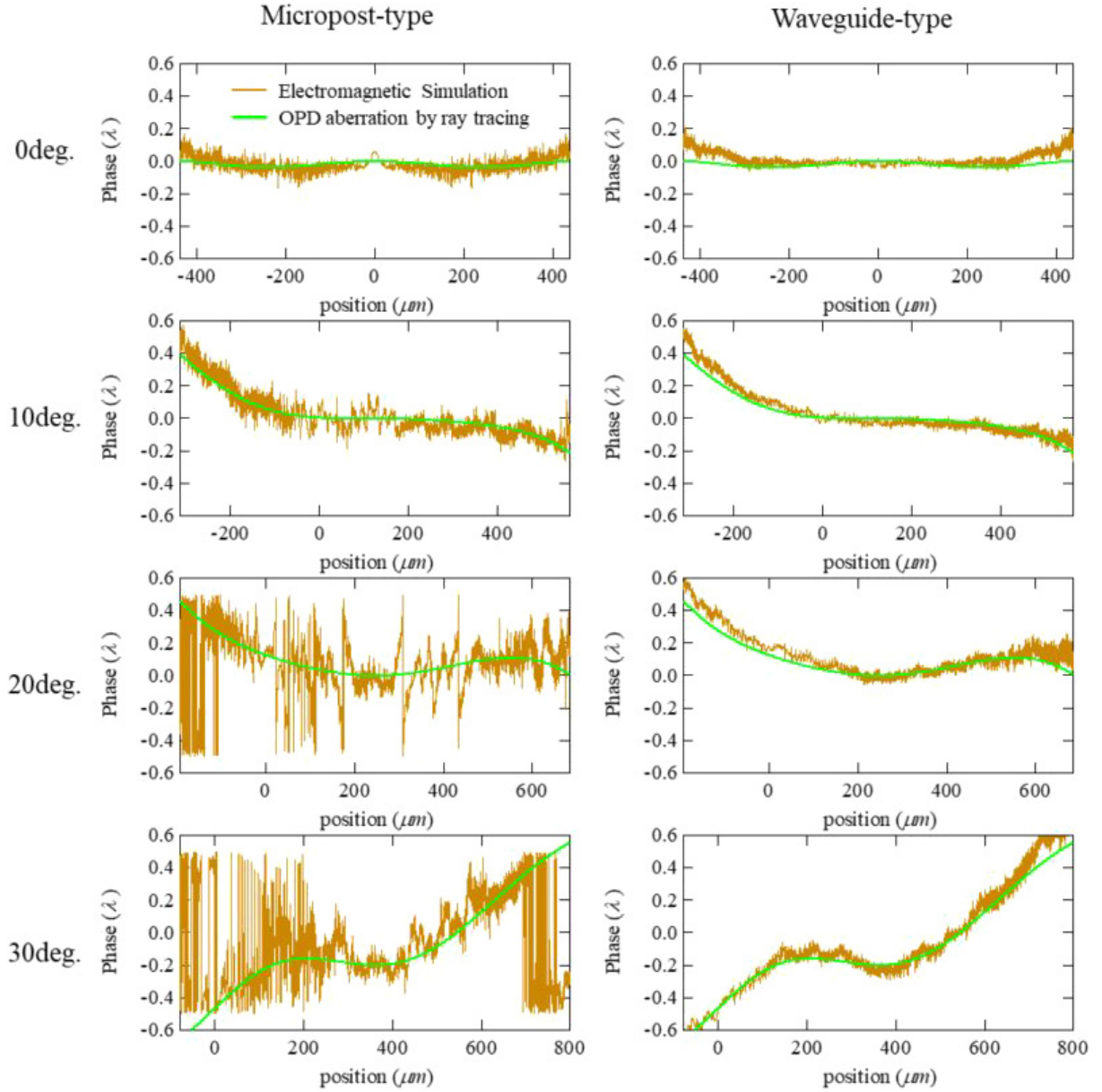


Fig. 8 Wavefront aberrations for each incident angle with TM polarization. Results for the micropost-type are shown in the left column, and those of the waveguide-type are in the right column. Electromagnetic simulations are plotted in light brown, and OPD aberrations are plotted in light green.

transform of the point-spread function. The speckle-like noise appears as flare under incoherent illumination.

Figs. 8 and 9 show the wavefront aberrations of the micropost-type and the waveguide-type. These are our main results. Fig. 8 is for TM polarization and Fig. 9 is for TE polarization. The left column is the micropost-type and the right column is the waveguide-type.

The light brown lines are the wavefront aberrations by electromagnetic field simulations that are the difference from the ideal spherical wavefront on the plane immediately after the focusing metalens. The green lines are the designed wavefront aberration calculated by ray tracing (CODE V, Synopsys, Inc.) as the optical path difference

(OPD) aberrations. Metalenses can be defined as phase profiles with even-order polynomials of the radial coordinate in ray tracing calculations. For the waveguide-type, it can be seen that the wavefronts of ray tracing and those of electromagnetic simulations are in good agreement in all cases. For the micropost-type, good agreement is shown when all the cases are of TE polarized light and also in the cases of TM polarized light at small angles of incidence. However, when the incident angle is as large as 20 deg and 30 deg, we can see very large fluctuations in the wavefront and large deviations from the wavefront by ray tracing. In this way, the waveguide-type can suppress the jaggedness of the wavefront aberrations for oblique incident TM polarized light.

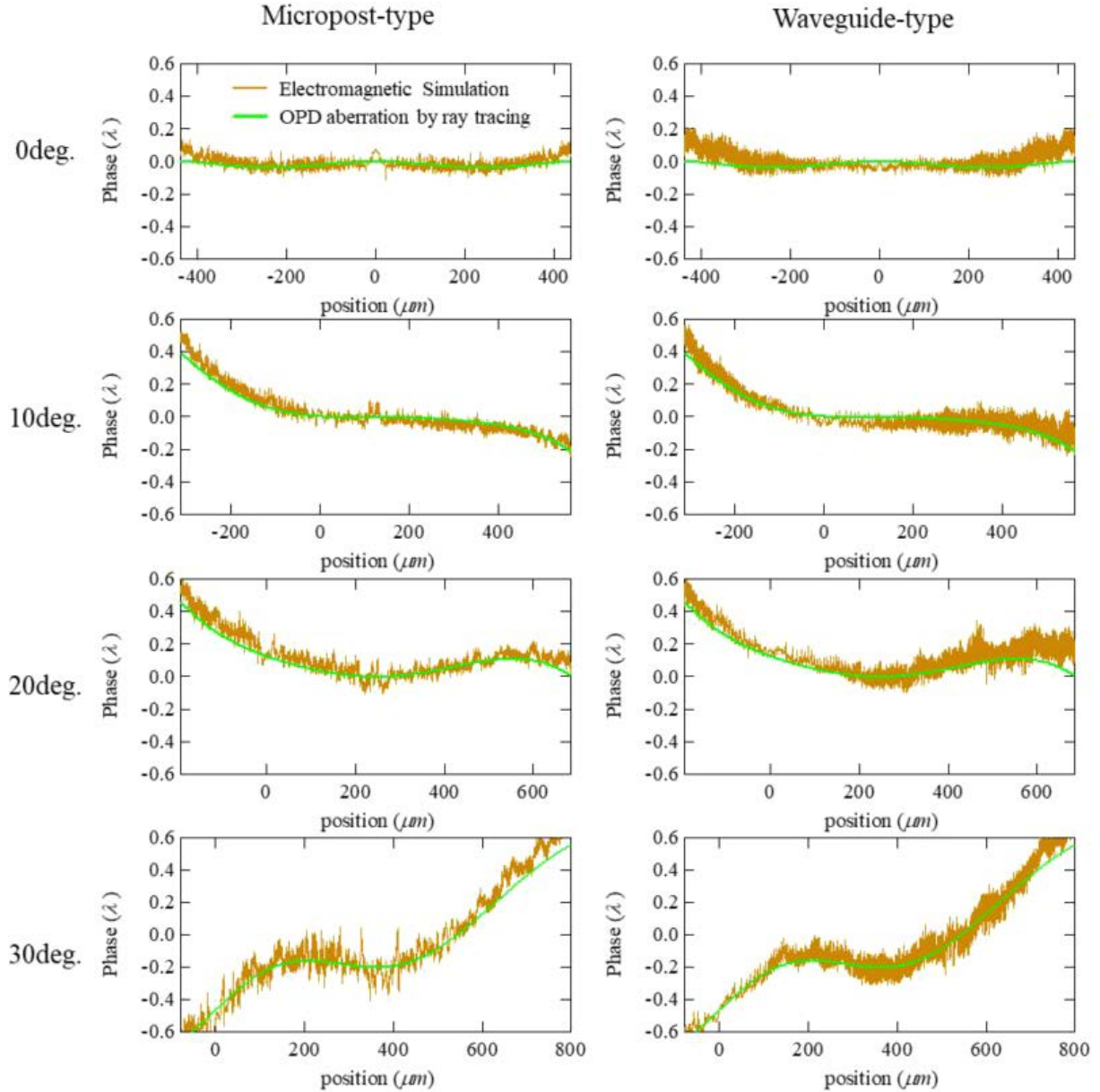


Fig. 9 Wavefront aberrations for each incident angle with TE polarization. Results for the micropost-type are shown in the left column, and those of the waveguide-type are in right column. Electromagnetic simulations are plotted in light brown, and OPD aberrations are plotted in light green.

The main difference between the micropost-type and the waveguide-type is whether it has multimode or single mode, as we can see in Fig. 3. Note that multimode can cause destructive interferences at oblique incidence. They can be seen in the results of the transmittance and transmission phase of the meta-atom itself at oblique incidence, as shown in Figs. 1 and 2, and can result in the jaggedness of the wavefront for the micropost-type metalens.

The difference between the two types can be clearly seen by looking at the wavefront aberration rather than the focal spots or MTF. In addition, the speckle-like noise that appeared at 20 deg and 30 deg of TM polarized light when discussing the MTF can be understood from the disturbance

of these wavefronts.

Fig. 10 shows the total power immediately after the correcting lens, the total power immediately after the focusing lens, and the focusing efficiency at the focus position when the power of the incident light on the correcting lens is unity. We define the focusing efficiency as the fraction of the incident light that focused within six times the FWHM spot size.

It can be seen that the focusing efficiencies of the waveguide-type are clearly better than those of the micropost-type. There is not a big difference between the waveguide-type and the micropost-type in terms of wavefront aberration for TE polarization (Fig. 9), but the focusing efficiencies are better than those of the micropost-type. From this result, it

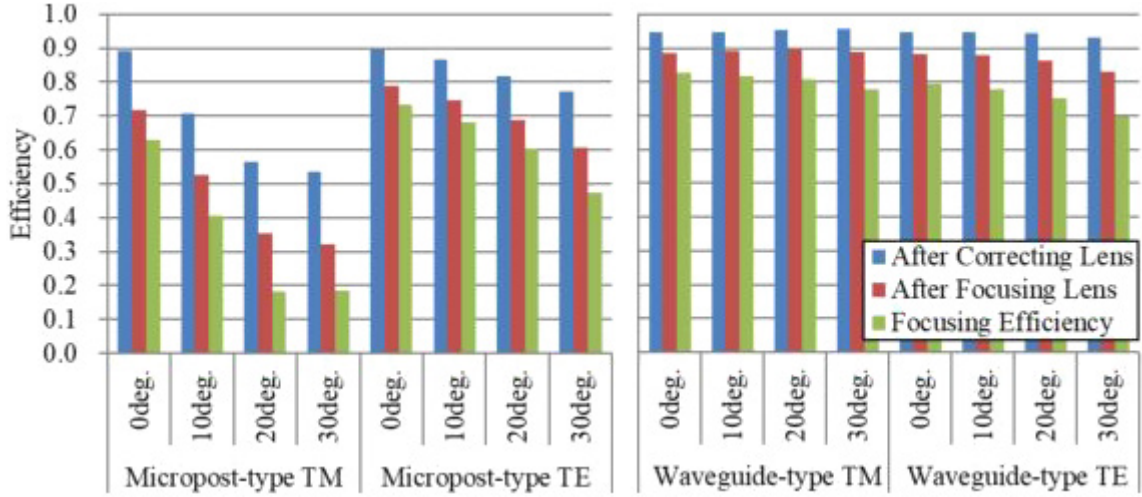


Fig. 10 Efficiency just after the two metasurfaces and focusing efficiencies for: (left) micropost-type doublet metalens and (right) waveguide-type doublet metalens.

is clear that the efficiencies are greatly improved using the waveguide-type metalens compared to the micropost-type metalens when the angle of incidence is large. As we mentioned above, in our simulations the multiple reflections will not have a significant effect if there is 10% reflection from a metasurface. All reflectance from each waveguide metalens are below 10%, except the condition when the incident angle is at 30 deg of TM polarized light whose reflectance for the focusing metalens is 11%; therefore, we can neglect the multiple reflections. As for the micropost-type, however, some reflectance for each metalens are more than 30% and multiple instances of reflected light may appear on the image plane as noise or flare. Therefore, the image quality for a micropost-type metalens can be worse in terms of multiple reflections.

5 Conclusion

It is shown that the wavefront aberrations estimated by full electromagnetic simulations for a waveguide-type metasurface are in good agreement with those found by ray tracing. On the other hand, when the incident angle is large, the wavefront of the micropost-type metalens has large fluctuations. Then, the difference from ray tracing becomes large and those fluctuations cause flare. These results show that the waveguide-type can improve the lens performance of Arbabi's doublet in terms of efficiency, wavefront aberration, and flare.

Because our simulations do not take fabrication errors into account, we cannot mention how tight the tolerance is. The waveguide-type structure is not easy to manufacture, and tight tolerance might be required, which will increase

the manufacturing costs. Therefore, a lens with nanodisk-type or micropost-type might be more desirable when using only normal incidence or when the incident angle is not so large. However, from our results, it is better to select the waveguide-type to make a metalens with a large angle of view for a single wavelength, which will have a small aberration and high efficiency. In addition, it is important to check whether the oblique incident characteristics meet the desired lens specifications when designing a sub-wavelength element.

APPENDIX A: Rayleigh–Sommerfeld Diffraction

Let's review the Rayleigh–Sommerfeld (RS) diffraction. When the medium is isotropic, homogeneous, and source free, the time-independent 3D Helmholtz equation for a single frequency is derived from Maxwell's equations:

$$\begin{aligned} (\nabla^2 + k^2)\mathbf{E}(\mathbf{x}) &= 0 \\ (\nabla^2 + k^2)\mathbf{H}(\mathbf{x}) &= 0 \end{aligned} \quad (\text{A.1})$$

where \mathbf{E} and \mathbf{H} are the electric and magnetic field, and k is wave number. From this formula, we know that each component of the electric or magnetic fields can be expressed independently from the other components. The Rayleigh–Sommerfeld formula of the first kind is

$$\begin{aligned} U(x, y) &= \int U(x', y') h(x - x', y - y') dx' dy' \\ h(x, y) &= \frac{\partial}{\partial z} \left(\frac{\exp(ik\sqrt{x^2 + y^2 + z^2})}{\sqrt{x^2 + y^2 + z^2}} \right) \end{aligned} \quad (\text{A.2})$$

where $U(x, y)$ is a complex amplitude of a field. It is an exact solution to the Helmholtz equation from an initial (x', y') plane

to a parallel (x, y) plane with distance z [20]. Therefore, if we know the six components of the electromagnetic field in an initial plane, we can independently calculate each field in the planes parallel to the initial plane using Eq. (A2). If the field distribution does not change along that y axis, as in our simulations, the Rayleigh–Sommerfeld formula in Eq. (A2) is reduced to

$$\begin{aligned} U(x) &= \int U(x')h(x-x')dx' \\ h(x) &= \frac{kz}{2i\sqrt{x^2+z^2}} H_1^{(2)}\left(k\sqrt{x^2+z^2}\right) \end{aligned} \quad (\text{A.3})$$

where $H_1^{(2)}$ is a Hankel function of the second kind.

Acknowledgment. The authors wish to thank Dr. Daniel G. Smith of Nikon Research Corporation of America, and Hironobu Makitsubo, Satoshi Yashiki, Hiroyuki Tsukamoto, Daisuke Mori, Hiroshi Konishi, and Seiki Yoshikawa of Nikon Corporation for their great help. Portions of this work were presented in 2021 at META 2021 as “Influence on wide-angle metasurface doublet due to different types of all-dielectric metasurface.”

References

- [1] P. Lalanne and P. Chavel, “Metalenses at visible wavelengths: past, present, perspectives,” *Laser Photon. Rev.* vol. 11, pp. 1600295, 2017.
- [2] P. Lalanne, S. Astilean, P. Chavel, E. Cambriil, and H. Launois, “Design and fabrication of blazed binary diffractive elements with sampling periods smaller than the structural cutoff,” *J. Opt. Soc. Am. A* vol. 16, pp. 1143–1156, 1999.
- [3] S. M. Kamali, A. Arbabi, E. Arbabi, Y. Horie, and A. Faraon, “Decoupling optical function and geometrical form using conformal flexible dielectric metasurfaces,” *Nat. Commun.* vol. 7, pp. 11618, 2016.
- [4] J. Cheng, D. Ansari-Oghol-Beig, and H. Mosallaei, “Wave manipulation with designer dielectric metasurfaces,” *Opt. Lett.* vol. 39, pp. 6285–6288, 2014.
- [5] M. Decker, I. Staude, M. Falkner, J. Dominguez, D. N. Neshev, I. Brener, T. Pertsch, and Y. S. Kivshar, “High-efficiency dielectric Huygens’ surfaces,” *Adv. Opt. Mater.* vol. 3, pp. 813–820, 2015.
- [6] A. Arbabi, E. Arbabi, S. M. Kamali, Y. Horie, S. Han, and A. Faraon, “Miniature optical planar camera based on a wide-angle metasurface doublet corrected for monochromatic aberrations,” *Nat. Commun.* vol. 7, pp. 13682, 2016.
- [7] C. Gigli, Q. Li, P. Chavel, G. Leo, M. L. Brongersma, and P. Lalanne, “Fundamental limitations of Huygens’ metasurfaces for optical beam shaping,” *Laser Photon. Rev.* vol. 15, pp. 2000448, 2021.
- [8] D. Arslan, K. E. Chong, D. N. Neshev, T. Pertsch, Y. S. Kivshar, and I. Staude, “Silicon Huygens’ metasurfaces at oblique incidence,” in *Conference on Lasers and Electro-Optics Europe European Quantum Electronics Conference*, 2017, paper EH_6_2
- [9] S. J. Byrnes, A. Lenef, F. Aieta, and F. Capasso, “Designing large, high-efficiency, high-numerical-aperture, transmissive meta-lenses for visible light,” *Opt. Express* vol. 24, pp. 5110–5124, 2016.
- [10] J. Yang and J. A. Fan, “Topology-optimized metasurfaces: impact of initial geometric layout,” *Opt. Lett.* vol. 42, pp. 3161–3164, 2017.
- [11] D. Sell, J. Yang, S. Doshay, R. Yang, and J. A. Fan, “Large-angle, multifunctional metagratings based on freeform multimode geometries,” *Nano Lett.* vol. 17, pp. 3752–3757, 2017.
- [12] M. G. Moharam and T. K. Gaylord, “Rigorous coupled-wave analysis of metallic surface-relief gratings,” *J. Opt. Soc. Am. A* vol. 3, pp. 1780–1787, 1986.
- [13] L. Li, “New formulation of the Fourier modal method for crossed surface-relief gratings,” *J. Opt. Soc. Am. A* vol. 14, pp. 2758–2767, 1997.
- [14] K. Yee, “Numerical solution of initial boundary value problems involving Maxwell’s equations in isotropic media,” *IEEE Trans. Antennas Propag.* vol. 14, pp. 302–307, 1966.
- [15] A. Taflove and S. C. Hagness, *Computational Electrodynamics: The Finite-difference Time-domain Method*, 3rd ed. Norwood: Artech House, 2005.
- [16] A. Arbabi, Y. Horie, A. J. Ball, M. Bagheri, and A. Faraon, “Subwavelength-thick lenses with high numerical apertures and large efficiency based on high-contrast transmittarrays,” *Nat. Commun.* vol. 6, pp. 7069, 2015.
- [17] C. Xu, M. Novak, D. Herrmann, L.-C. Hu, E. Heller, and M. Bahl, “Effective approach for design and simulation of metalens structures,” in *META 2019 Lisbon—Portugal The 10th International Conference on Metamaterials, Photonic Crystals and Plasmonics*, 2019, pp. 1828.
- [18] F. Aieta, M. A. Kats, P. Genevet, and F. Capasso, “Multi-wavelength achromatic metasurfaces by dispersive phase compensation,” *Science* vol. 347, pp. 1342–1345, 2015.
- [19] F. Shen and A. Wang, “Fast-Fourier-transform based numerical integration method for the Rayleigh–Sommerfeld diffraction formula,” *Appl. Opt.* vol. 45, pp. 1102–1110, 2006.
- [20] L. Mandel and E. Wolf, *Optical Coherence and Quantum Optics*, Cambridge: Cambridge University, 1995.
- [21] H. Toba, H. Takagi, M. Ohashi, K. Otaki, and Y. Takigawa, “Influence on wide-angle doublet metalenses due to different types of all-dielectric metasurfaces,” *Appl. Opt.* vol. 61, pp. 597–606, 2022.

鳥羽英光 Hidemitsu TOBA
光学本部 要素開発部
Fundamental Technology Development Department
Optical Engineering Division

高木英嗣 Hidetsugu TAKAGI
光学本部 第一設計部
1st Designing Department
Optical Engineering Division

大橋道雄 Michio OHASHI
光学本部 第二設計部
2nd Designing Department
Optical Engineering Division

大滝 桂 Katsura OTAKI
光学本部 要素開発部
Fundamental Technology Development Department
Optical Engineering Division

瀧川雄一 Yuichi TAKIGAWA
光学本部 要素開発部
Fundamental Technology Development Department
Optical Engineering Division